Stochastic gravitational wave background from smoothed cosmic string loops

Jose J. Blanco-Pillado and Ken D. Olum

Phys. Rev. D **96**, 104046 — Published 27 November 2017

DOI: 10.1103/PhysRevD.96.104046

Stochastic gravitational wave background from smoothed cosmic string loops

Jose J. Blanco-Pillado*

Department of Theoretical Physics, University of the Basque Country, Bilbao, Spain and IKERBASQUE, Basque Foundation for Science, 48011, Bilbao, Spain

Ken D. Olum†

Institute of Cosmology, Department of Physics and Astronomy, Tufts University, Medford, MA 02155, USA

Abstract

We do a start-to-finish calculation of the stochastic gravitational wave background to be expected from cosmic strings. We start from a population of string loops taken from simulations, smooth these by Lorentzian convolution as a model of gravitational back reaction, calculate the average spectrum of gravitational waves emitted by the string population at any given time, and propagate it through a standard model cosmology to find the stochastic background today. Except for modeling back reaction as smoothing, we take into account all known effects, including changes in the number of cosmological relativistic degrees of freedom at early times and the possibility that some energy is in rare bursts that we might never have observed.

* josejuan.blanco@ehu.es

† kdo@cosmos.phy.tufts.edu

I. INTRODUCTION

Our universe may contain a network of cosmic strings, which could be either flux tubes arising from a symmetry-breaking transition at high energies or the fundamental strings of superstring theory (or one-dimensional D-branes) stretched out to astrophysical lengths [1–3]. The best way to discover such a network, if it exists, is to observe the stochastic background of gravitational waves emitted by cosmic string loops. Non-observation of such a background in pulsar timing arrays currently gives the strongest bounds on the energy scale of a possible cosmic string network.

In usual models, cosmic strings do not have ends. Thus they exist as a "network" of infinite strings and closed loops. Intersections between strings lead to reconnections, and when a string intersects itself, it produces a loop. Loops then oscillate relativistically and decay by the emission of gravitational waves. If the string energy per unit length is μ, the gravitational power emitted is $\Gamma G\mu$, where Γ is a number of order 50 depending on the shape of the string, and G is Newton's constant. We work in units where $c = 1$.

In both the matter and the radiation era, the flow of energy from long strings into loops and thence into gravitational waves maintains the network in a scaling regime, where all linear measures, such as the average distance between strings, stay at a fixed multiple of the horizon distance (or the age of the universe). Scaling allows us to extrapolate over many orders of magnitude between what can be studied in a simulation and the universe today.

To connect observations or observational limits to the properties of possible cosmic strings, we need to accurately compute the spectrum of gravitational waves to be expected from a cosmic string network of a given energy scale. The steps in this process are as follows.

1. First we simulate the network of cosmic strings to find the rate of production of loops of various sizes from the long string network, and we extract a representative sample of loop shapes from the simulation.

2. This gives the distribution of loop shapes at the time the loops are formed, but gravitational back reaction modifies these shapes. Since we do not yet have a code for calculating these changes in shape, we use a toy model of smoothing to estimate them.

3. We then compute the gravitational spectrum and total power Γ for each loop.

4. Using Γ, which also gives the evaporation rate, we integrate the production and evaporation processes over cosmological time to determine the distribution of loops existing at each redshift z.

5. We integrate the spectrum of individual loops over the loop distribution at each z to find the overall emission spectrum.

6. Then we integrate the emission spectrum over cosmological time to get the present-day background.

Items 1, 2, and 4 have already been done in Refs. [4–6]. The purpose of this paper is to complete the program with items 3, 5, and 6. We include all known effects except that we use a smoothing model rather than computing directly the effects of gravitational back reaction on loop shapes. A companion paper compares the results with current observations [7].

It is traditional in papers such as this to consider "small loop" models in which the predominant size of loops at production is $\Gamma G\mu$ times the production time, so loops last for only about one Hubble time. In our opinion, there is no reason to consider such models any more. They were inspired by early simulations [8, 9] that found loops at the resolution scale, but recent simulations [4, 10–14], with much greater reach, found loop production at scales related to the horizon size at the time of production.

In this work we consider local cosmic strings (those which do not have any long-range forces or couplings to massless particles other than the graviton) that do not have vertices where 3 or more strings join. This includes Abelian-Higgs strings and fundamental superstrings, but not axion strings, non-Abelian gauge strings, or (p, q) superstrings.

We model these strings using the Nambu approximation of a linelike relativistic string, as in Refs. [4, 8–15]. This is an extremely good approximation even in the Abelian-Higgs case. The present-day ratio of loop size or curvature scale, $\Gamma G\mu t_0$, to the string thickness, about $\sqrt{\mu/\hbar}$, is $\Gamma(G\mu)^{(3/2)}t_0/t_{\rm Planck} \sim 10^{44}$. Thus on any possible scale relevant to field theory dynamics, strings are straight to fantastically good approximation, and their motion should be given by the Nambu-Goto equations of motion. Indeed this was shown to be the case in simulations of individual Abelian-Higgs strings when the curvature scale was larger than the thickness [16–18].

Many calculations of gravitational waves from cosmic strings have been done before. Ref. [19] made the first estimate of the background from strings, using a simple scaling distribution of horizon size loops radiating in the fundamental mode, and Ref. [20] used a similar analysis to generate a bound based on pulsar timing. Ref. [21] calculated the background using all modes in the spectrum of simple loops. Refs. [22–24] derived bounds based using the "small loop" models suggested by simulations at the time, and Refs. [23, 24] included the changes in the number of relativistic degrees of freedom. Refs. [25–27] introduced the possibility of low intercommutation probability appropriate to cosmic superstrings and compared the results with the capabilities of modern interferometric gravitational wave detectors. Refs. [28–32] explored a wide range of different scenarios of loop sizes, power spectrum, and intercommutation probability, and investigated the implications for several current and projected observatories. In [6] we used the number density distribution of loops from the latest numerical simulations, in the approximation that all radiated power is due to cusps. In the present paper we will use not only the number density but the shapes of loops found in simulations.

Refs. [33–36] analyzed bursts coming from cosmic string cusps and their potential observability.

The remainder of this paper is structured as follows. In the next section we calculate the gravitational wave background in terms of the expansion history of the universe, the distribution of loops at each epoch, and the power spectrum of gravitational waves emitted from a typical loop. We discuss these three components in turn in Secs. III, IV, and V. Sec. VI gives our results, and we conclude in Sec. VII.

Some technical matters are deferred to appendices. Appendix A gives the details of the calculation of the radiated power from a cusp. Appendix B discusses how many harmonics need to be computed to find the spectrum in any given direction. Appendix C discusses summing contributions from the discrete modes emitted by loops, and Appendix D considers whether the fact that some power is in very rare bursts requires a modification of the stochastic background calculation.

II. STOCHASTIC GRAVITATIONAL WAVE BACKGROUND

We will compute the stochastic background of gravitational waves presently existing as the fraction of the critical density given by the energy of gravitational waves in unit logarithmic interval of frequency,[1]

$$\Omega_{\rm gw}(\ln f) = \frac{8\pi G}{3H_0^2} f \rho_{\rm gw}(t_0, f)\,, \tag{2}$$

where $\rho_{\rm gw}$ is the energy density in gravitational waves per unit frequency. Since gravitational waves persist from very early times, the energy in a comoving region is just the redshifted total energy deposited there,

$$\rho_{\rm gw}(t_0, f) = \int_0^{t_0} \frac{dt}{(1+z(t))^4} P_{\rm gw}(t, f') \frac{\partial f'}{\partial f}\,, \tag{3}$$

where $P_{\rm gw}(t, f')$ is the total gravitational wave power of all loops existing at time t into unit range of emitted frequencies. The emitted frequency that becomes frequency f today is just $f' = (1+z)f$, so we find

$$\rho_{\rm gw}(t_0, f) = \int_0^{t_0} \frac{dt}{(1+z(t))^3} P_{\rm gw}\left(t, (1+z)f\right). \tag{4}$$

Consider one loop of length l existing at time t. It emits gravitational waves at a set of discrete frequencies. Radiation in harmonic n is emitted at frequency $f' = 2n/l$, and there is a discrete power spectrum P_n, giving the power in each harmonic, in units of $G\mu^2$. Each loop has its own spectrum, but we will use the loops we get from simulations to produce an average spectrum and then treat all loops as emitting with that spectrum.

To find $P_{\rm gw}(t, f')$, we sum over the contributions coming from all n. For each n there is a specific length of loop, $l = 2n/f'$, that gives frequency f' in that harmonic. Let $\mathsf{n}(l, t)$ be the number density per unit length interval of loops of length l existing at time t. Then

$$P_{\rm gw}(t, f') = G\mu^2 \sum_{n=1}^{\infty} \mathsf{n}(l, t) \frac{dl}{df'} P_n = G\mu^2 \sum_{n=1}^{\infty} \frac{2n}{f'^2} \mathsf{n}(l, t) P_n\,. \tag{5}$$

Thus we can write

$$\rho_{\rm gw}(t, f) = G\mu^2 \sum_{n=1}^{\infty} C_n P_n\,, \tag{6}$$

[1] The same background can be expressed as its power spectral density,

$$S_h(f) = \frac{3H_0^2}{2\pi^2 f^3} \Omega_{\rm gw}(\ln f)\,, \tag{1}$$

or as its characteristic strain $h_c = \sqrt{f S_h(f)}$. Pulsar timing arrays use these quantities directly, but interferometers adjust them by averaging interferometer sensitivity over polarization and arrival direction, reducing S_h by 5 and h_c by $\sqrt{5}$ over the values given here. For a clear explanation of various measures of the background see Ref. [37].

with

$$C_n(f) = \int_0^{t_0} \frac{dt}{(1+z)^5} \frac{2n}{f^2} \mathsf{n}(l,t)\,. \tag{7}$$

We can now change the integration variable using

$$dt = -\frac{dz}{H(z)(1+z)} \tag{8}$$

to get

$$C_n(f) = \frac{2n}{f^2} \int_0^{\infty} \frac{dz}{H(z)(1+z)^6}\, \mathsf{n}\left(\frac{2n}{(1+z)f}, t(z)\right) \tag{9}$$

Equations (6,9) give the stochastic background in terms of the cosmology ($H(z), t(z)$), the loop density $\mathsf{n}(l,t)$, and the radiation power spectrum of each loop, P_n. In the following, we will discuss these effects in turn.

III. COSMOLOGY

The cosmological dependence in Eq. (9) is in $H(z)$ in the denominator and $t(z)$ appearing as an argument to the loop distribution $\mathsf{n}(l,t)$. We will consider a flat radiation + matter + Λ cosmology, with

$$H(z) = H_0 \sqrt{\Omega_\Lambda + (1+z)^3 \Omega_m + G(z)(1+z)^4 \Omega_r}\,, \tag{10}$$

where the function

$$G(z) = \frac{T(z)^4 g_*(z)}{T_0^4 (1+z)^4 g_{*,0}} \tag{11}$$

corrects for the change in the number of relativistic degrees of freedom at early times. Here $T(z)$ is the temperature at redshift z, $g_*(z)$ the effective number of relativistic degrees of freedom then, and T_0 and $g_{*,0}$ these quantities today.

Neutrinos today are presumably nonrelativistic and should technically be included in Ω_m and not Ω_r. But the value of Ω_r is important only at early times when neutrinos were relativistic. So we define Ω_r here to be the value it would have with massless neutrinos of temperature (because neutrino decoupling takes place before electron-positron annihilation) $(4/11)^{1/3}$ times the present cosmic microwave background temperature.

The age of the universe at redshift z is the integral of Eq. (8),

$$t(z) = \int_z^{\infty} \frac{dz'}{H(z')(1+z')}\,, \tag{12}$$

where we will use [38]

$$\Omega_\Lambda = 0.69\,, \tag{13a}$$

$$\Omega_m = 0.31\,, \tag{13b}$$

and we can compute

$$\Omega_r = \frac{32\pi G\sigma g_{*,0} T_0^4}{3H_0^2}\,, \tag{14}$$

where σ is the Stefan-Boltzmann constant, and $g_{*,0} \approx 3.36$ is the effective number of relativistic degrees of freedom with photons and massless neutrinos. With $T_0 = 2.2725K$ and writing $H_0 = 100h$ km/s/Mpc as usual, we find

$$h^2\Omega_r = 4.15 \times 10^{-5}\,. \tag{15}$$

When necessary we will use the value $h = 0.68$ [38].

IV. LOOP DENSITY

A. Uniform radiation era

Reference [6] gives an analytic approximation to the number density of loops in the radiation era,

$$\mathsf{n}_r(l,t) = \frac{0.18}{t^{3/2}\left(l + \Gamma G\mu t\right)^{5/2}} \tag{16}$$

for $l < 0.1t$. The loop density at any given time is an integral over the previous loop production. In the radiation era, the integrand is sharply peaked and so it is quite accurate to treat the loop production as a δ-function in loop size whose position and amplitude are chosen to match simulation results, leading to Eq. (16). For details see Ref. [6].

Equation (16) applies when the universe has been in the radiation era (without changes in the degrees of freedom) for a long time. Accordingly it exhibits scaling behavior in which

$$\mathsf{n}_r(l,t) = t^{-4}\mathsf{n}(x)\,, \tag{17}$$

where $x = l/t$ and $\mathsf{n}(x)$ is the number of loops per unit x in volume t^3,

$$\mathsf{n}(x) = \frac{0.18}{\left(x + \Gamma G\mu\right)^{5/2}}\,. \tag{18}$$

In this case, there is a simple result. Deep in the radiation era, and ignoring changes in the degrees of freedom,

$$H(z) = (1+z)^2 H_r \,, \tag{19}$$

$$t(z) = \frac{1}{2(1+z)^2 H_r} \,, \tag{20}$$

where

$$H_r = H_0 \sqrt{\Omega_r} \tag{21}$$

is the contribution from radiation to the Hubble constant today.

Putting Eq. (19) into Eq. (9) gives

$$C_n(f) = \frac{2n}{f^2} \int \frac{dz}{(1+z)^8 H_r} \; \mathsf{n}\left(\frac{2n}{(1+z)f}, t(z) \right) \,. \tag{22}$$

We use Eq. (17) to change from $\mathsf{n}(l,t)$ to $\mathsf{n}(x)$, with t given by Eq. (20), to get

$$C_n(f) = \frac{32 H_r^3}{f^2} \int dz \, \mathsf{n}(x) \,. \tag{23}$$

Then we change the variable of integration from z to

$$x = \frac{l}{t} = \frac{8n(1+z)H_r}{f} \,, \tag{24}$$

giving

$$C_n(f) = \frac{8 H_r^2}{f} \int dx \, \mathsf{n}(x) \,. \tag{25}$$

From Eq. (25), we see that C_n has no dependence on n, so the stochastic background depends only on

$$\Gamma = \sum_{n=1}^{\infty} P_n \,, \tag{26}$$

that C_n depends only on the total loop number density[2] in volume t^3,

$$\int_0^\infty dx \, \mathsf{n}(x) = 0.12 (\Gamma G \mu)^{-3/2} \,, \tag{27}$$

and finally that $C_n(f) \sim 1/f$, so the power per unit logarithmic interval of frequency, $\Omega_{\rm gw}(\ln f)$, is constant.

Using Eqs. (2,6,25,26,27), we find

$$\Omega_{\rm gw}(\ln f) = 8.0 \Omega_r \sqrt{\frac{G\mu}{\Gamma}} \,, \tag{28}$$

[2] This agrees with Eq. (21) of Ref. [6], which gives the number in volume $d_h^3 = 8t^3$

and Eq. (15) gives

$$h^2\Omega_{\rm gw}(\ln f) = 3.3\times10^{-4}\sqrt{\frac{G\mu}{\Gamma}} = 4.7\times10^{-5}\sqrt{G\mu}\,, \tag{29}$$

with $\Gamma = 50$.

The high-frequency background comes almost entirely from deep in the radiation era, so one might expect a plateau in $\Omega_{\rm gw}(\ln f)$ given by Eq. (29). However, we will see below that changes in the number of degrees of freedom introduce a few smooth steps on this plateau region of the spectrum.

B. Changes in the number of degrees of freedom

At early times, the expansion rate of the universe changes because of the annihilation of relativistic species, which injects additional energy into the universe and reduces its rate of cooling. These changes are incorporated into the function $G(z)$ of Eq. (11). We handle them as follows.

We do not consider changes to the scaling properties of the string network, but assume that it always traces the current rate of expansion. But we do take into account the fact that the important loops at any given time are relics of earlier times when $G(z)$ was different.

First consider a universe which spends a long time in a radiation era with $G(z) = G_1$. Instead of Eqs. (19,20), we have

$$H(z) = (1+z)^2 H_r\sqrt{G_1} \tag{30}$$

and

$$t(z) = \frac{1}{2(1+z)^2 H_r\sqrt{G_1}}\,. \tag{31}$$

The loop density is still given by Eq. (16), with t from Eq. (31),

$$\mathsf{n}_r(l,t) = \frac{0.18\cdot 2^{3/2}(H_r^2 G_1)^{3/4}(1+z)^3}{(l+\Gamma G\mu t)^{5/2}} \tag{32}$$

and

$$l = \frac{2n}{(1+z)f}\,. \tag{33}$$

We will use Eq. (32) even in the case where $G(z)$ is changing, although this is not entirely accurate. Taking into account more effects would lead to an even smoother dependence of $\Omega_{\rm gw}$ on f.

Once loops of a certain size are no longer being produced in significant numbers, their density merely dilutes, going as $(1+z)^3$, and the loops become shorter by gravitational back reaction. Both these processes are included in Eq. (32), so Eq. (32) holds for in any later era, with G_1 always being the $G(z)$ at the time at which the loop was produced.

Of course not all loops of the same size were produced at the same time, but the loop production function is peaked in a fairly narrow range of loop size to production time ratio around 0.1 [6], so we will make this approximation to compute G_1. Suppose a loop with length l at time t was produced at time t_1. Then its length at production was $l+\Gamma G\mu(t-t_1)$ and its ratio of length to production time was

$$x_1 = \frac{l + \Gamma G\mu(t - t_1)}{t_1} \,. \tag{34}$$

Setting $x_1 = 0.1$ and using the approximation $\Gamma G\mu \ll x_1$, we find

$$t_1 \approx 10(l + \Gamma G\mu t) \,. \tag{35}$$

and then

$$G_1 = G(z(t_1)) \,. \tag{36}$$

We compute $G(z)$ using a code for $g_*(z)$ written by Masaki Yamada, which includes the contributions from all the particles in the Standard Model. The result is to introduce small steps in the $G(z)$ function, noticeable especially around electron-positron annihilation and the QCD phase transition.

Putting Eq. (32) in Eq. (9) gives

$$C_n(f) = \frac{0.18 \cdot 2^{5/2} H_r^{3/2} n}{f^2} \int dz \frac{G_1(l,t)^{3/4}}{H(z)(1+z)^3 \left(l + \Gamma G\mu t\right)^{5/2}} \,, \tag{37}$$

where z is the redshift at which the gravitational wave is emitted, $t = t(z)$ is the age of the universe at redshift z, given by Eq. (20) in the radiation era after electron-positron annihilation, l is given by by Eq. (33), and $G_1(l,t)$ is computed using Eqs. (35,36).

C. Matter era

In the matter era, there are two kinds of loops. For $G\mu$ compatible with observational bounds, the most important loops were formed in the radiation era. Their density is given

by Eq. (32), which already includes dilution as the universe expands and loss of length due to gravitational radiation. We thus use Eq. (37) in all eras, with $H(z)$ and $t(z)$ as appropriate.

With t in the matter era and $G\mu$ around current limits, we can set $G_1 = 1$, although we do not make this approximation in our numerical calculations. The largest loops formed at the time of electron-positron annihilation have size about $0.1t_{\rm ep}$. For them to survive until matter-radiation equality at $t_{\rm eq}$ requires $\Gamma G\mu t_{\rm eq} < 0.1t_{\rm ep}$ and thus $\Gamma G\mu < 0.1t_{\rm ep}/t_{\rm eq} \approx 6 \times 10^{-13}$, or $G\mu \lesssim 10^{-14}$.

There are also loops formed in the matter era. Analysis of simulations [6] gives the density of such loops in a scaling regime,

$$\mathsf{n}_m(l,t) = \frac{0.27 - 0.45(l/t)^{0.31}}{t^2\,(l + \Gamma G\mu t)^2} \tag{38}$$

for $l < 0.18t$. Loop production in the matter era is not so strongly peaked as in the radiation era. Equation (38) is the result of a two-parameter analytic fit to the loop production seen in simulations. For details see Ref. [6]

Using Eq. (38) in Eqs. (6,9) gives the stochastic background arising from these loops. We give the result in Sec. VI, but it is negligible compared to the background from relic loops from the radiation era. The basic reason is that for the dominant loop size $l \sim \Gamma G\mu t$, Eq. (16) is larger than Eq. (38) by factor $(\Gamma G\mu)^{-1/2}$. For $G\mu < 2 \times 10^{-11}$, this is at least 2×10^5.

We did not study loops formed during the matter to radiation transition. But these also have little consequence. In fact, even loops formed near the end of the radiation era make little contribution. From Eqs. (31,35) and taking $t_0 H_0 \approx 1$, $G_1 = 1$, and using Eq. (15), we find the dominant loops today were produced at redshift about

$$0.16\Omega_r^{-1/4}(\Gamma G\mu)^{-1/2} \approx 16(\Gamma G\mu)^{-1/2} > 5 \times 10^5 \tag{39}$$

for $G\mu < 2 \times 10^{-11}$. This is far larger than the redshift of matter-radiation equality, about 3000.

V. SPECTRUM OF A LOOP

A. Population of loops

The last ingredient is P_n, the average gravitational spectrum radiated from a loop. We compute this separately for loops formed in the matter era and those formed in the radiation era. In each case, we use a sample of loops found in simulations. (See Ref. [4] for a discussion of simulation techniques.). We used 1060 loops in the radiation era and 812 in the matter era.

These simulation loops, however, are not representative of loops existing at any given time, because those loops have lost a significant fraction of their energy due to gravitational wave emission and thus have had their shapes modified by back reaction. For the present paper, we model this effect by smoothing the loops by convolving them with a Lorentzian [5], even though we know [39, 40] that this model is not entirely correct. We consider the last three smoothing steps, corresponding to loss of 1/8, 1/4, and 1/2 of the initial loop length. In the next section we give some separate results for these three steps, but for the final result we used only the last step. Including the others would not make any noticeable difference.

Convolution yields a set of smooth loops whose radiation power P_n we would like to compute. We should not model these loops in a piecewise linear form, as we do for loops in our simulations. A piecewise linear loop would have kinks between the pieces, and at sufficiently high frequencies these fictitious kinks could make a big difference to the gravitational radiation power.

Instead, we represent the strings as smooth functions given by their Fourier transforms. We keep the Fourier amplitudes for some finite number N_f (up to 4096) of frequencies. To compute the gravitational radiation spectrum of such loops, we must understand their motion, which we now discuss.

B. Loop motion and cusps

The expansion of the universe is very important for the evolution of the string network and later for the propagation of gravitational waves. But the loops we will study are always much smaller than the Hubble distance, and so their evolution takes place essentially in flat

space.

The general solution for the motion of a Nambu-Goto string in flat spacetime can be written

$$X^\mu(t,\sigma) = \frac{1}{2}\left[X^\mu_-(\sigma_-) + X^\mu_+(\sigma_+)\right] , \tag{40}$$

where $\sigma_\pm = t \pm \sigma$, are the lightcone coordinates on the string worldsheet built from the timelike coordinate t and the spacelike parameter σ. We will work in the gauge where the 4-vector functions $X^\mu_\pm$ have $X^0_\pm = \sigma_\pm$, and the spatial part obeys the constraints $|\mathbf{X}'_-(\sigma_-)| = |\mathbf{X}'_+(\sigma_+)| = 1$, where, as usual, the prime denotes a derivative of the function with respect to its argument. The two functions $\mathbf{X}_\pm$ specify the motion of the loop. It is these functions that we smooth to emulate gravitational back reaction effects, and it is these smooth functions that we represent by their Fourier coefficients.

For a closed loop in the rest frame, $\mathbf{X}_\pm$ are periodic, $\mathbf{X}_\pm(\sigma_\pm) = \mathbf{X}_\pm(\sigma_\pm + l)$, and thus

$$\int_0^l \mathbf{X}'_\pm(\sigma_\pm) d\sigma_\pm = 0 \, . \tag{41}$$

Thus $\mathbf{X}'_+$ and $\mathbf{X}'_-$ each trace out a loop on the "Kibble-Turok" unit sphere [41–43], and the center of gravity of the loop is at the center of the sphere. Generically these two paths will cross, so there are usually points where

$$\mathbf{X}'_+(\sigma^c_+) = \mathbf{X}'_-(\sigma^c_-) \, . \tag{42}$$

Thus at $t_c = (\sigma^c_+ + \sigma^c_-)/2$, $\sigma_c = (\sigma^c_+ - \sigma^c_-)/2$, the string velocity (formally) reaches the speed of light,

$$\left|\frac{d\mathbf{X}}{dt}\right| = 1 \, , \tag{43}$$

and the string doubles back on itself,

$$\frac{d\mathbf{X}}{d\sigma} = 0 \, , \tag{44}$$

so such a point is called a cusp.[3]

The existence of cusps leads to difficulties in computing the gravitational radiation spectrum from a loop. When there is a cusp, the spectrum falls only as $n^{-4/3}$ [21], where n is the harmonic number of the radiation. Thus the integrated power falls only as $n^{-1/3}$. This slow

[3] Note that cusps are not artifacts of Nambu-Goto dynamics. In fact they are formed in field theory cosmic strings, as we showed [16] in the Abelian-Higgs model.

decrease makes it impractical to accurate compute the total power by simply computing numerically up to some maximum n. Instead we compute the power from cusps analytically (See Appendix A), and use this computation for high frequencies in directions near cusps.

Cosmic strings may also have kinks: places where there is a discontinuous change in $\mathbf{X}'$. These lead to a spectrum which falls as $n^{-5/3}$ [43]. However, in the present analysis, kinks are smoothed out by convolution, so that we do not have to consider them in our computations. A better analysis of kink evolution [39] show that kinks are opened out rather than being rounded off. In future work we will compute the actual back reaction numerically, but at the moment we are restricted to modeling it as a smoothing process.

C. Radiation power

Computation of the radiation power spectrum, P_n, for each of our loops proceeds as follows. First we find cusps, the places where the paths of $\mathbf{X}'_+$ and $\mathbf{X}'_-$ cross on the unit sphere. We do this by generating by fast Fourier transform (FFT) at least $10N_f$ samples of each function and looking for crossings between the great-circle paths connecting adjacent samples. When we find such a crossing, we narrow it down using the Fourier transform representations of $\mathbf{X}_\pm$.

Then we integrate the gravitational radiation power over solid angle by dividing the sphere of emission directions into triangles. We start with an icosahedron projected onto the sphere and then repeatedly divide each triangle into 4 smaller triangles by inserting a point at the center of each edge [44]. If we perform the division process $N_{\rm split}$ times, the total number of triangles is $20 \times 4^{N_{\rm split}}$. We used $N_{\rm split} = 5$.

We now see how close each triangle comes to the direction (i.e., the $\mathbf{X}'_+ = \mathbf{X}'_-$) of any cusp. If there is a cusp inside the triangle or within a threshold angle, taken as 0.1, we compute the emission using the cusp emission procedure described Sec. V E below. If not, we compute the radiation using the generic expression for the power given in Sec. V D in the direction of the center of the triangle (given by the normalized average of the 3 corner directions) and multiply by the area of the triangle on the unit sphere.

D. Radiation in a generic direction

To compute the radiation power in a given direction $\hat{\mathbf{\Omega}}$, we follow Refs. [45–47]. The goal of this section is the same as that of Ref. [46], but here we benefit from much larger simulations enabled by 25 years of improvement in computer power, and we deal with smoothed loops rather than those taken directly from simulations.

The angular power density emitted in harmonic n is

$$\frac{dP_n}{d\Omega} = \frac{G\mu^2 l^2}{2\pi}\omega_n^2(|A_+|^2 + |A_\times|^2) = 8\pi G\mu^2 n^2(|A_+|^2 + |A_\times|^2)\,, \tag{45}$$

where l is the length of the loop, $\omega = 4\pi n/l$ and A_+ and $A_\times$ are the amplitudes of the two gravitational wave polarizations. If we construct a coordinate system whose z axis is in the $\hat{\mathbf{\Omega}}$ direction, they are given by

$$A_+ = I_x^- I_x^+ - I_y^- I_y^+\,, \tag{46a}$$

$$A_\times = I_y^- I_x^+ + I_x^- I_y^+\,, \tag{46b}$$

where

$$\mathbf{I}^{\pm(n)}(\hat{\mathbf{\Omega}}) = \frac{1}{l}\int_0^l d\sigma_\pm\, \mathbf{X}'_\pm(\sigma_\pm) e^{(2\pi i n/l)(\sigma_\pm - X_z(\sigma_\pm))}\,. \tag{47}$$

From Eqs. (46) we find

$$|A_+|^2 = |I_x^-|^2|I_x^+|^2 + |I_y^-|^2|I_y^+|^2 - 2\,\mathrm{Re}(I_x^- I_y^{-*} I_x^+ I_y^{+*})\,, \tag{48}$$

$$|A_\times|^2 = |I_y^-|^2|I_x^+|^2 + |I_x^-|^2|I_y^+|^2 + 2\,\mathrm{Re}(I_x^{-*} I_y^- I_x^+ I_y^{+*})\,, \tag{49}$$

where asterisk means complex conjugation. Thus

$$|A_+|^2 + |A_\times|^2 = |I_\perp^-|^2|I_\perp^+|^2 + 4\,\mathrm{Im}(I_x^- I_y^{-*})\,\mathrm{Im}(I_x^+ I_y^{+*})\,, \tag{50}$$

where $|I_\perp^\pm|^2 = |I_x^\pm|^2 + |I_y^\pm|^2$. We can write

$$\mathrm{Im}(I_x^\pm I_y^{\pm *}) = (\mathbf{I}_I \times \mathbf{I}_R)_z\,, \tag{51}$$

where the subscripts I and R mean the imaginary and real parts of the vector. This shows that the result is independent of the choice of the coordinate system in the perpendicular plane.

We would now like to compute $\mathbf{I}_\perp^{\pm(n)}$ in directions far from any cusp, for specific $\mathbf{X}_\pm$ given in terms of their Fourier transforms. To do this quickly, we would like to use FFT

to compute all necessary n at once. However, Eq. (47) does not have the form of a Fourier transform, because the exponent is not simply $2\pi i n\sigma_\pm/l$. But we can approximate it as a nonuniform discrete Fourier transform as follows.

First take N positions $\sigma_j = jL/N$, $j = 0 \ldots N-1$. To compute I_x^+, for example, we generate $X'_x(\sigma_j)$ and $\phi_j = (\sigma_j - X_z^+(\sigma_j))/l$ at these N positions. This can be done by FFT using the Fourier components of X_x^+. We then have

$$I_x^{+(n)}(\hat{\mathbf{\Omega}}) = \frac{1}{N}\sum_{j=0}^{N-1} X_x'^{+}(\sigma_j) e^{2\pi i n\phi_j} \,. \tag{52}$$

This is a non-uniform Fourier transform problem, which can be solved in $O(N \ln N)$ time. We use the method of Potts, Steidl, and Tasche [48]. The choice of how many n to compute is discussed in Appendix B.

E. Radiation in a cusp direction

In the case where the triangle is close to the direction of the cusp, the situation is more difficult. In any given direction the gravitational power from the cusp decreases with frequency only as $\omega^{-2/3}$, so the power per logarithmic interval of ω increases as $\omega^{1/3}$. This continues until the radiation is cut off at some maximum frequency proportional to θ^{-3}, where θ is the angle between the cusp direction and the direction of observation. The angular area over which a given frequency ω is important is proportional to $\theta^2 \sim \omega^{-2/3}$, so the radiation from a cusp, integrated over solid angle, declines as $\omega^{-4/3}$ and the contribution per logarithmic interval goes as $\omega^{-1/3}$.

This long tail makes it difficult to compute the radiation accurately using the techniques above. First, we would need huge numbers of harmonics near the cusp, and second, the high-frequency radiation varies rapidly over small distances within the triangle. To solve this problem, we calculate the high-frequency cusp radiation analytically using a simple model of the cusp, and then integrate numerically over the triangular region.

Because this model does not work well for low frequencies, we compute those using Eqs. (45-47) even in the direction of the cusps. Because of aliasing, FFT techniques do not give accurate answers even at low frequencies, unless all frequencies with significant power are included. So we compute the integral in Eq. (47) directly. The decision of which

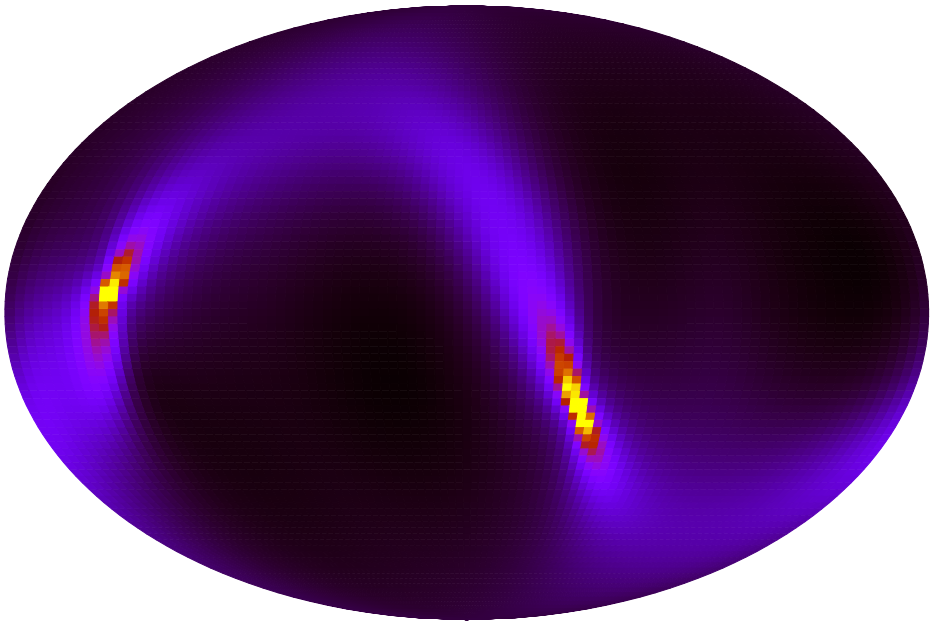

FIG. 1. Spatial distribution of the gravitational radiation from a smooth loop. We show the Mollweide projection of the radiation density on a sphere surrounding the loop. The brighter regions represent the high radiation density in the direction of the cusps.

frequencies are done by which technique is made by using the cusp technique whenever the frequency would have significant variation over the range of directions in the triangle.

The details of the cusp procedure are given in Appendix A. We show in Fig. 1 an example of the radiation density emitted by a typical loop. We see the enhancement of the radiation density along the directions of the cusps.

VI. RESULTS

A. Total radiation power Γ of a loop

The simplest result that one can obtain is the total radiation power, integrated over directions and frequencies. This has the form $P = \Gamma G\mu^2$, so the goal is to determine the constant Γ. The slowest known radiator is the Allen-Casper-Ottewill (ACO) loop [49] studied extensively by Anderson [50–52], with $\Gamma \approx 39.0025$. There is no upper limit to Γ. For example, the Γ of Burden [45] loops grows without bound as the angle between the

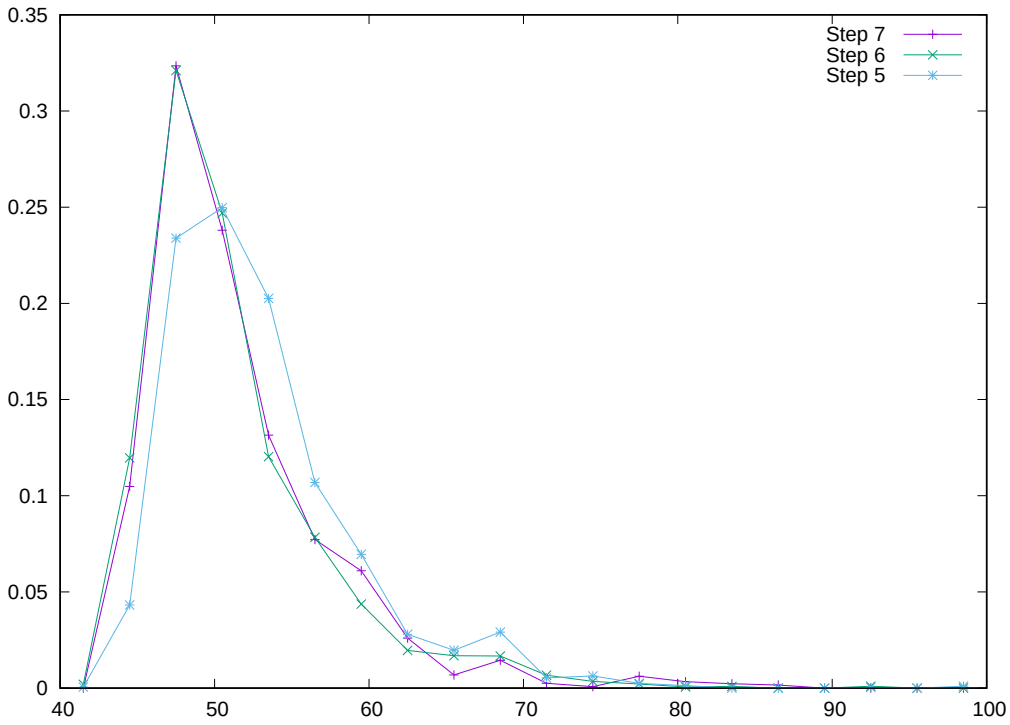

FIG. 2. Histogram of Γ values for the loops in the radiation era at various stages of smoothing. The results for the matter era are very similar.

planes of $\mathbf{X}^+$ and $\mathbf{X}^-$ decreases. The power spectrum and the total power emitted from these loops can be computed using the expressions found in [45]. We have used these simple loop solutions as test beds for our numerical code. The results are in very good agreement with the analytic calculations.

A histogram of Γ for loops taken from simulations with various degrees of smoothing is shown in Fig. 2. Remarkably, for the great majority of loops, $\Gamma \sim 50$. Since smoothing the loop produces cusps that were not there before, one might think that smoother loops would have higher radiation power. However, as shown in Fig. 3, the additional power emitted by the cusp comes at the expense of non-cusp emission. Thus the presence of cusps moves the power to higher frequencies but produces little change in the overall power.

Consequently it is a good approximation to use $\Gamma = 50$ always, and we do not need to concern ourselves with the fact that different loops evaporate at different rates. We have calculated the average value of Γ for a population of 1060 loops obtained in 3 radiation era runs and obtained $\bar{\Gamma}_r = 51.43$.

In the matter era we consider 812 loops and the average total radiation power is $\bar{\Gamma}_m =$

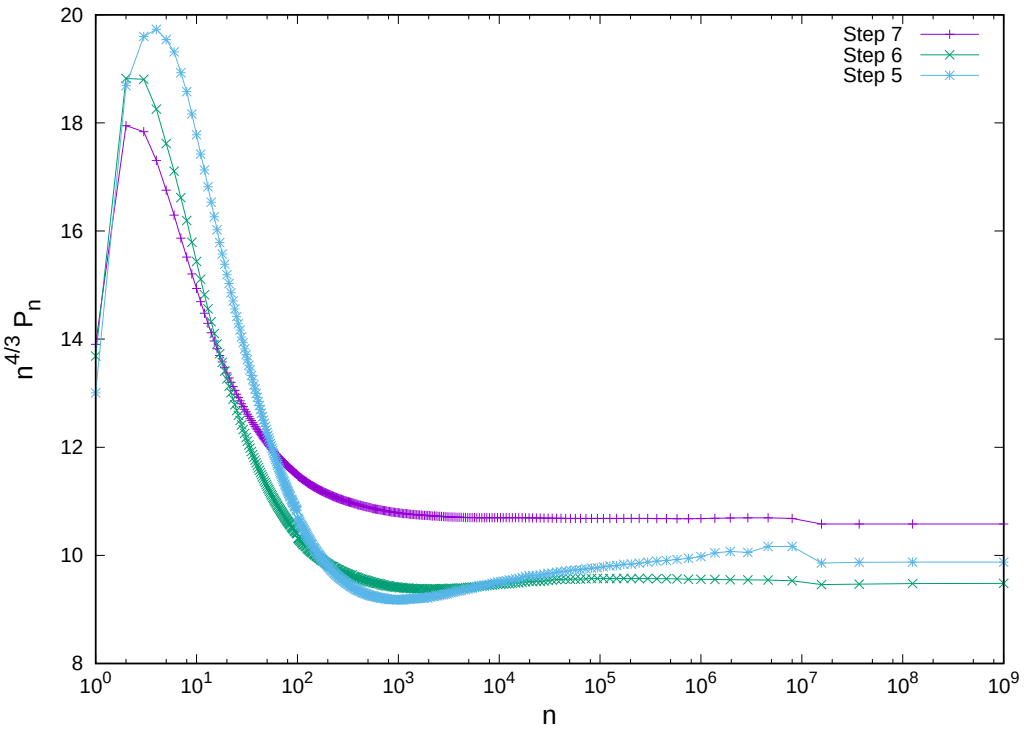

FIG. 3. Average power spectrum scaled by $n^{4/3}$ of radiation era loops at three stages of smoothing. The feature at $n \approx 10^7$ is an artifact. See the end of Appendix B

53.55.

B. Power spectrum

The power spectrum of the loop is the set of discrete numbers P_n, $n = 1 \ldots \infty$. We use this spectrum in Eq. (6) to compute $\rho_{\rm gw}(f)$ and so $\Omega_{\rm gw}(\ln f)$. But of course we cannot compute an infinite set of numbers. Instead we compute a finite number of P_n, with the n chosen to give an accurate result in $\rho_{\rm gw}(f)$, taking account of our expectation that P_n will drop as $n^{-4/3}$. The details are given in Appendix C. We take a weighted average[4] of the P_n of the smoothed loops from the simulation to use in Eq. (6). The average P_n for loops in the radiation and matter eras are shown in Fig. 4.

We note that even though the average power spectrum is very smooth, some of the loops have quite different shapes, which leads to some variety in the power spectra as shown in

[4] See Ref. [5] for a detailed description of the weighting procedure to compute the averages from our sample of loops from the simulation.

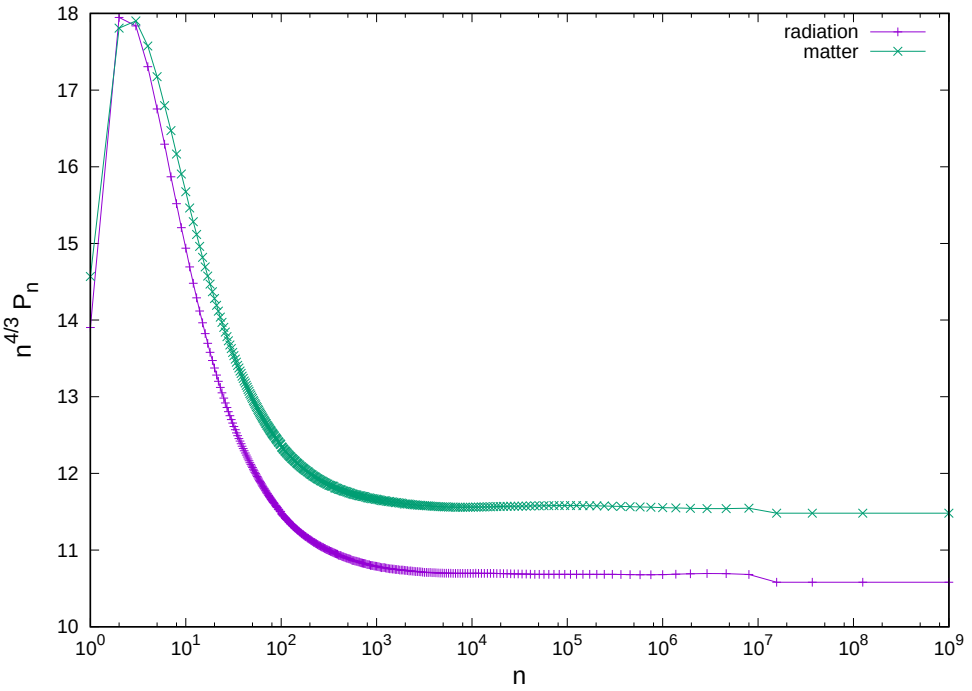

FIG. 4. Average power spectrum scaled by $n^{4/3}$ of radiation and matter era loops. We show here only the power spectrum at the last step on the smoothing procedure. See the end of Appendix B for a discussion of the artifact at $n \approx 10^7$

Fig. 5. Of course this variation is amplified by the way we choose to represent the power spectrum by $n^{4/3}P_n$.

C. Stochastic Gravitational Wave Spectrum: $\Omega_{\mathbf{gw}}(\ln f)$

With the P_n, and the C_n from Eq. (9) using the loop densities computed in Sec. IV, we compute $\Omega_{\rm gw}(\ln f)$ for a range of frequencies f using Eqs. (2,6). The results are shown in Fig. 6. This includes the contributions from the loops in all the eras, as described earlier in the text.

The general form of the spectra can be understood as follows. Very low frequencies can only be emitted by large loops, but large loops are suppressed by $l^{-5/2}$, as in Eq. (16). There is an extra power of f in Eq. (2), so at very low frequencies, $\Omega_{\rm gw}$ goes as $f^{-3/2}$. At even lower frequencies there is a cutoff because there are essentially no strings of size $l > 0.1t$ at time t, but this does not appear in Fig. 6.

At high frequencies, we are sensitive only to loops radiating in the radiation era. Ac-

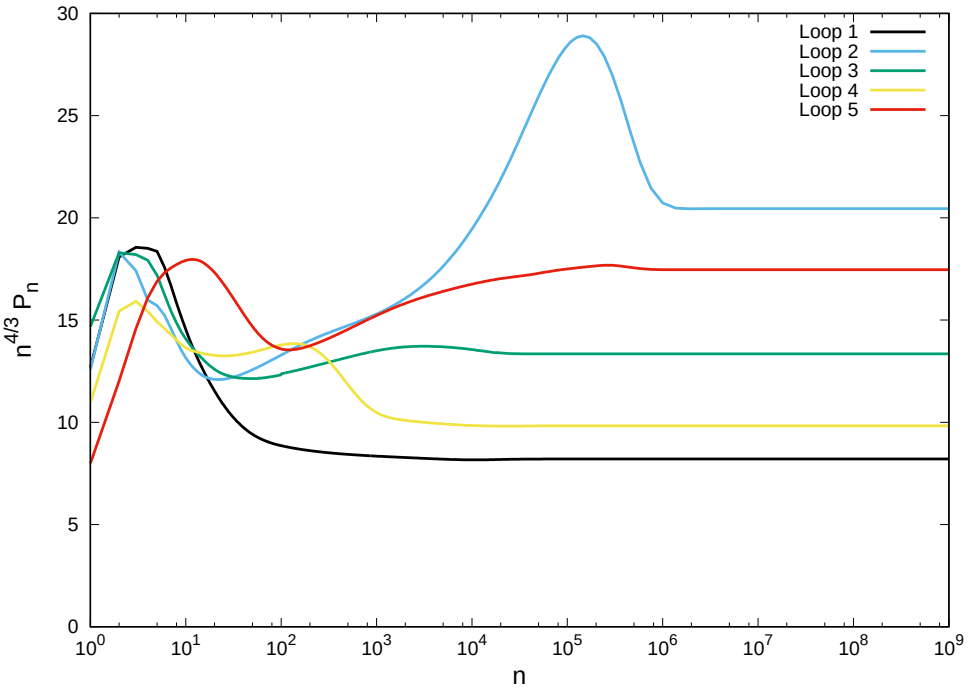

FIG. 5. Power spectra of a few individual loops in the radiation era, chosen to show the diversity of possibilities. The great majority of loops have spectra similar to loop 1 here, but some are quite different. Nevertheless, averaging over many loops gives the smooth spectra shown in Fig. 4.

cording to Eq. (29) this would give a plateau proportional to $\sqrt{G\mu}$. However, changes in the number of relativistic degrees of freedom at early times turn the plateau into a series of decreasing plateaus, which are smoothed into a decline with some wiggles.[5] At intermediate frequencies is there is a peak resulting from gravitational wave emission in the matter era.

Decreasing $G\mu$ does not change the frequencies at which any given loop radiates, but the overall power drops proportionately to $G\mu$. Simultaneously, the lower $G\mu$ allows loops to survive longer, so that at any given time there is now a new, larger population of older and smaller loops, which radiate at higher frequencies. The net result is that the curve of $\Omega_{\rm gw}$ moves downward proportionately to $\sqrt{G\mu}$ and to the right as $1/(G\mu)$.

To model intercommutation probability $p < 1$ in the standard way one should move up the graph for the desired $G\mu$ by factor $1/p$. However, we feel that more work is needed to understand low-p string networks. While increasing the loop density by $1/p$ reproduces the

[5] Note that adding new ingredients in the thermal history of the universe, such as new physics beyond the Standard Model, could introduce new features in this spectrum. In principle, detecting this stochastic background from strings could allow us to probe the thermal history of the universe, though in fact the effect occurs only at very high frequencies

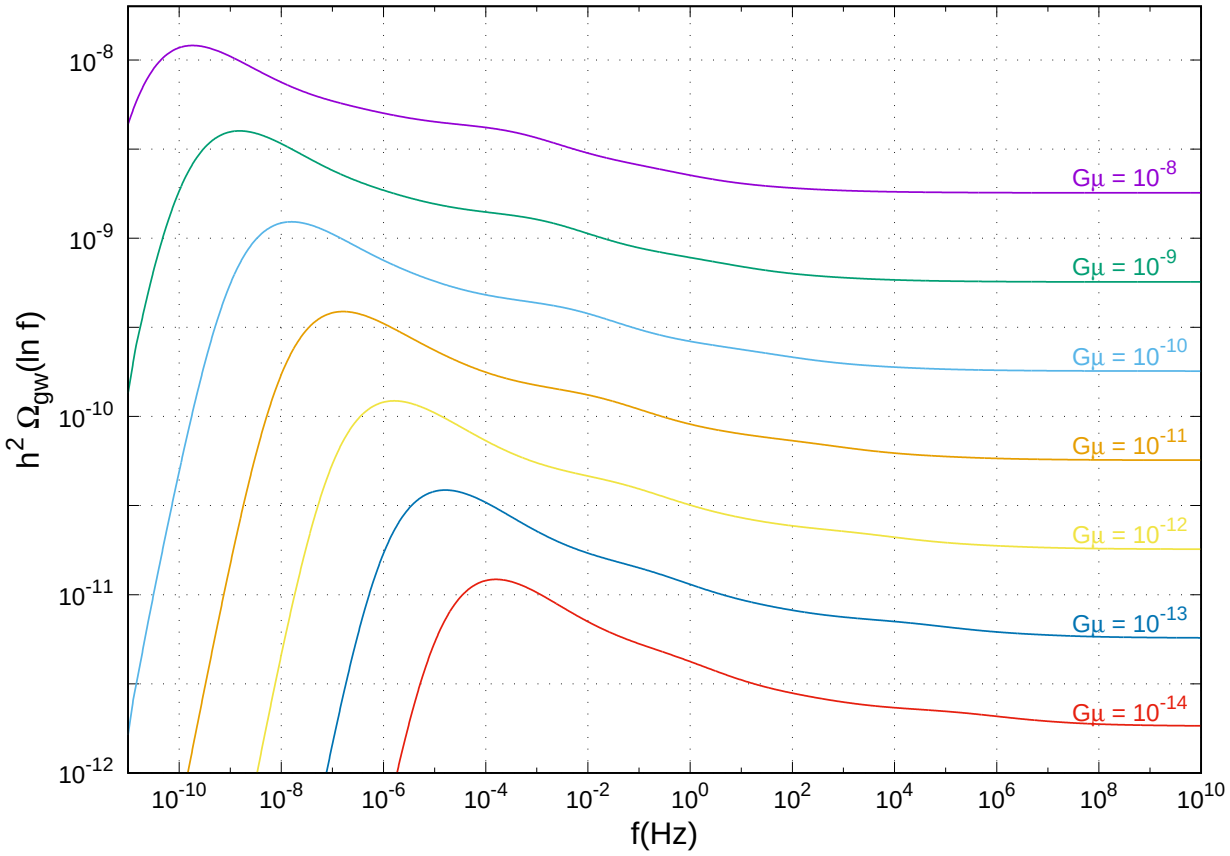

FIG. 6. The stochastic gravitational wave spectrum for string tensions between $G\mu = 10^{-8}$ and 10^{-14}.

$p = 1$ average reconnection rate between unrelated strings, the production of loops requires a long string to intersect with itself, and the chance of that is unaffected by the overall density. So the evolution of a $p < 1$ network may be more complicated than a simple rescaling.

VII. CONCLUSION

We have computed the stochastic background of gravitational waves to be expected from a network of local cosmic strings with $G\mu$ ranging from 10^{-8} to 10^{-14}. We used a ΛCDM cosmology with string loops taken from simulations and smoothed by Lorentzian convolution as a model of gravitational backreaction [5]. We analyzed strings in the radiation era, strings from the radiation era radiating in the matter era, and strings produced in the matter era (though these, and all strings in the recent Λ-dominated era, make no essentially no contribution). We took account of changes in the number of relativistic degrees of freedom

in the very early universe, which give an important reduction in the background at high frequencies. We found (see Appendix D) that there is no need remove energy contained in rare bursts from the observable stochastic background. The only missing ingredient is a real calculation of gravitational backreaction, which the subject of work currently in progress.

A companion paper [7] compares the results predicted here with limits from current observations and discusses the prospects of detection in the future. The data shown in Fig. 6, with the range $G\mu$ extended down to 10^{-25}, are available at
`http://cosmos.phy.tufts.edu/cosmic-string-spectra/`.

ACKNOWLEDGMENTS

We thank Masaki Yamada for providing us with a code to compute the g_* function, and Xavier Siemens and Alex Vilenkin for helpful conversations. This work was supported in part by the National Science Foundation under grant numbers 1213888, 1213930, 1518742, and 1520792. J. J. B.-P. is supported in part by the Basque Foundation for Science (IKERBASQUE), the Spanish Ministry MINECO grant (FPA2015-64041-C2-1P) and Basque Government grant (IT-979-16).

Appendix A: Gravitational wave power from cusps

In this appendix we compute the gravitational radiation power due to the string near a cusp in directions close to the direction in which the cusp is moving, $\mathbf{X}_+ = \mathbf{X}_-$. The idea of the analysis is very similar to Refs.[33–36], but those analyses were interested in the waveform for burst detection, whereas here we need the power spectrum to compute the stochastic background. We also compute the power spectrum for cusps with specific parameters rather than what is expected for a generic cusp.

To simplify the calculation, we will choose our coordinate system so that the z axis lies in this direction (note that this is a different convention from that of Sec. V), and the y axis lies perpendicular to both the cusp direction and the observation direction, which we can thus write

$$\hat{\mathbf{\Omega}} = (\sin\theta, 0, \cos\theta)\,, \tag{A1}$$

where θ is the angle between cusp and observation directions.

We put the point of the cusp at $\sigma_\pm = 0$, and expand the string around that point,

$$\mathbf{X}_+(\sigma_+) = \sigma_+\hat{\mathbf{z}} + \frac{1}{2}\mathbf{x}''_+\sigma_+^2 + \frac{1}{6}\mathbf{x}'''_+\sigma_+^3 \tag{A2a}$$

and

$$\mathbf{X}_-(\sigma_-) = \sigma_-\hat{\mathbf{z}} + \frac{1}{2}\mathbf{x}''_-\sigma_-^2 + \frac{1}{6}\mathbf{x}'''_-\sigma_-^3\,, \tag{A2b}$$

where we defined $\mathbf{x}''_\pm = \mathbf{X}''_-(0)$ and $\mathbf{x}'''_\pm = \mathbf{X}'''_-(0)$. The constraints of the equations of motion require that

$$\mathbf{x}_z^{\pm\prime\prime} = 0\,, \tag{A3}$$

and

$$\mathbf{x}_z^{\pm\prime\prime\prime} = -|\mathbf{x}''_\pm|^2\,. \tag{A4}$$

We ignore other components of $\mathbf{x}'''$, which contribute only at higher orders in θ, so Eqs. (A2) become

$$\mathbf{X}_\pm(\sigma_\pm) = \sigma_\pm\hat{\mathbf{z}} + \frac{1}{2}\mathbf{x}''_\pm\sigma_\pm^2 - \frac{1}{6}|\mathbf{x}''_\pm|^2\sigma_\pm^3\hat{\mathbf{z}}\,, \tag{A5}$$

and Eq. (47) can be written

$$\mathbf{I}^\pm = \frac{1}{l}\int_0^l \mathbf{X}'_\pm e^{(i/2)(\omega\sigma_\pm - \mathbf{k}\cdot\mathbf{X}_\pm)}d\sigma_\pm\,, \tag{A6}$$

where ω is the frequency of the emitted radiation and $k = \omega\hat{\mathbf{\Omega}}$ is its wavevector.

To describe the polarization of the gravitational waves, we need two unit vectors lying in the plane perpendicular to $\hat{\mathbf{\Omega}}$. We choose

$$\hat{\mathbf{n}}_1 = (\cos\theta, 0, -\sin\theta)\ , \tag{A7}$$

$$\hat{\mathbf{n}}_2 = \hat{\mathbf{y}}\,. \tag{A8}$$

We use Eqs. (45,50) and convert from discrete to continuous frequencies with $\omega = 4\pi n/l$ to get the spectral power density

$$\frac{dP}{d\omega d\Omega} = \frac{G\mu^2 l^3\omega^2}{8\pi^2}\left[|I_\perp^+|^2|I_\perp^-|^2 + 4\,\mathrm{Im}\,I_1^- I_2^{-*}\,\mathrm{Im}\,I_1^+ I_2^{+*}\right]\ , \tag{A9}$$

where $I_i^\pm = I^\pm(\mathbf{n}_i) = \mathbf{n}_i\cdot\mathbf{I}^\pm$ and $|I_\perp^\pm|^2 = |I_1^\pm|^2 + |I_2^\pm|^2$.

Since we are interested in the radiation near the cusp, we expand $\mathbf{n}_i$ and $\mathbf{k}$ in the small parameter θ to get

$$\mathbf{k} = \omega\left(\theta, 0, 1-\theta^2/2\right) \tag{A10}$$

$$\hat{\mathbf{n}}_1 = \left(1-\theta^2/2, 0, -\theta\right) \tag{A11}$$

$$\hat{\mathbf{n}}_2 = (0,1,0)\ . \tag{A12}$$

Using Eqs. (A2),

$$I^{\pm}(\hat{\mathbf{n}}) = \frac{1}{l}\int_0^l (\hat{\mathbf{n}}_z + \sigma_{\pm}(\mathbf{x}''_{\pm}\cdot\hat{\mathbf{n}}))e^{(i\omega/4)\left(\theta^2\sigma_{\pm} - (\mathbf{k}\cdot\mathbf{x}''_{\pm})\sigma_{\pm}^2 + |\mathbf{x}''_{\pm}|^2\sigma_{\pm}^3/3\right)}\, d\sigma_{\pm}\,. \tag{A13}$$

Using Eq. (A3), the second derivatives of the $\mathbf{X}^{\pm}$ at the cusp can always be written

$$\mathbf{x}''_{-}(\sigma_{-}) = (\alpha_{-}\cos\phi_{-})\hat{\mathbf{x}} + (\alpha_{-}\sin\phi_{-})\hat{\mathbf{y}} \tag{A14}$$

and similarly,

$$\mathbf{x}''_{+}(\sigma_{+}) = (\alpha_{+}\cos\phi_{+})\hat{\mathbf{x}} + (\alpha_{+}\sin\phi_{+})\hat{\mathbf{y}}\,, \tag{A15}$$

giving

$$I^{\pm}(\hat{\mathbf{n}}) = \frac{1}{l}\int_0^l (Q_{\pm}(\hat{\mathbf{n}}) + P_{\pm}(\hat{\mathbf{n}})\sigma_{\pm})\; e^{i\left(A_{\pm}\sigma_{\pm} + B_{\pm}\sigma_{\pm}^2 + C_{\pm}\sigma_{\pm}^3\right)}\, d\sigma_{\pm}\,, \tag{A16}$$

where

$$Q_{\pm}(\hat{\mathbf{n}}_1) = \hat{\mathbf{z}}\cdot\mathbf{n}_1 = -\theta \tag{A17}$$

$$P_{\pm}(\hat{\mathbf{n}}_1) = \mathbf{x}''_{\pm}\cdot\mathbf{n}_1 = \alpha_{\pm}\cos\phi_{\pm} \tag{A18}$$

$$Q_{\pm}(\hat{\mathbf{n}}_2) = \hat{\mathbf{z}}\cdot\mathbf{n}_2 = 0 \tag{A19}$$

$$P_{\pm}(\hat{\mathbf{n}}_2) = \mathbf{x}''_{\pm}\cdot\mathbf{n}_2 = \alpha_{\pm}\sin\phi_{\pm} \tag{A20}$$

$$A_{\pm} = \frac{\omega\theta^2}{4} \tag{A21}$$

$$B_{\pm} = -\frac{\omega\theta}{4}\alpha_{\pm}\cos\phi_{\pm} \tag{A22}$$

$$C_{\pm} = \frac{\omega}{12}\alpha_{\pm}^2\,, \tag{A23}$$

and where we kept only the lowest order in θ in each term. The integral in Eq. (A16) can be done in closed form, giving

$$I_1^{\pm} = I^{\pm}(\hat{\mathbf{n}}_1) = e^{-i\Phi_{\pm}}\left[\frac{2}{\sqrt{3}}\frac{\theta^2}{\alpha_{\pm}l}\sin^2\phi_{\pm}\left(i\cos\phi_{\pm}K_{2/3}(\xi_{\pm}) - |\sin\phi_{\pm}|K_{1/3}(\xi_{\pm})\right)\right] \tag{A24}$$

$$I_2^{\pm} = I^{\pm}(\hat{\mathbf{n}}_2) = e^{-i\Phi_{\pm}}\left[\frac{2}{\sqrt{3}}\frac{\theta^2}{\alpha_{\pm}l}\sin\phi_{\pm}|\sin\phi_{\pm}|\left(i|\sin\phi_{\pm}|K_{2/3}(\xi_{\pm}) + \cos\phi_{\pm}K_{1/3}(\xi_{\pm})\right)\right], \tag{A25}$$

where $\Phi_{\pm}$ are some irrelevant phases,

$$\xi_{\pm} = \frac{1}{6}\omega\theta^3\frac{|\sin^3\phi_{\pm}|}{\alpha_{\pm}}\,, \tag{A26}$$

and K is the modified Bessel function. Thus

$$|I_1^{\pm}|^2 + |I_2^{\pm}|^2 = \frac{4}{3}\frac{\theta^4}{\alpha_{\pm}^2 l^2}\sin^4\phi_{\pm}\left(K_{1/3}(\xi_{\pm})^2 + K_{2/3}^2(\xi_{\pm})\right) \tag{A27}$$

$$\mathrm{Im}\, I_1^{\pm} I_2^{\pm} = \frac{4}{3}\frac{\theta^4}{\alpha_{\pm}^2 l^2}\sin^4\phi_{\pm}\,\mathrm{sign}(\sin\phi_{\pm})K_{1/3}(\xi_{\pm})K_{2/3}(\xi_{\pm})\,. \tag{A28}$$

Putting these in Eq. (A9), we find

$$\frac{dP}{d\omega d\Omega} = \frac{2G\mu^2\omega^2\theta^8}{9\pi^2 l}\frac{\sin^4\phi_+\sin^4\phi_-}{\alpha_+^2\alpha_-^2}\Big[\left(K_{1/3}^2(\xi_+)+K_{2/3}^2(\xi_+)\right)\left(K_{1/3}^2(\xi_-)+K_{2/3}^2(\xi_-)\right) \quad \text{(A29)}$$
$$+4\,\mathrm{sign}(\sin\phi_+\sin\phi_-)K_{1/3}(\xi_+)K_{2/3}(\xi_+)K_{1/3}(\xi_-)K_{2/3}(\xi_-)\Big].$$

Note that this expression gives the power emitted by the cusp per frequency and per solid angle as a function of the the length of the loop and four parameters that describe the cusp, namely $(\alpha_\pm, \phi_\pm)$, which describe the crossing of the vectors $\mathbf{X}'_+$ and $\mathbf{X}'_-$ on the Kibble-Turok sphere and the relative angle with respect to the observation direction. Our code to compute the power spectrum from individual loops in the simulation first looks at the possible cusps in each loop and identifies these parameters. We can then integrate Eq. (A29) over solid angle and over ranges of frequency to include in the gravitational radiation spectrum from triangles that are near cusps.

We do not use it for low frequencies where the approximation of the set of discrete harmonics by the continuous frequency ω would lead to significant inaccuracy.

Appendix B: The number of harmonics to compute

Except for directions near cusps, we find the power spectrum by computing $I_\pm^{(n)}$ by fast Fourier transform. This yields all harmonics up through some maximum $n_{\max}$. In most directions, the power falls quickly, and we only need to compute a few harmonics. But in directions close to any $\mathbf{X}'_\pm$, the corresponding $I_\pm^{(n)}$ may fall very slowly. We estimate how many harmonics we need to compute for any given direction as follows.

We consider the computation of $I_x^{+(n)}$ and suppress all + subscripts and superscripts for this section. We define

$$f(\sigma) = \sigma - X_z(\sigma) \quad \text{(B1)}$$

$$g(\sigma) = X'_x(\sigma) \quad \text{(B2)}$$

$$h(\sigma) = f'(\sigma) = 1 - X'_z(\sigma) \quad \text{(B3)}$$

so that

$$I_x^{(n)} = \frac{1}{l}\int_0^l d\sigma\, g(\sigma)e^{i\varpi_n f(\sigma)}\,, \quad \text{(B4)}$$

with $\varpi_n = 2\pi n/l$. We can set the origin of coordinates so that $\mathbf{x}(0) = 0$. Then as σ goes from 0 to l, $f(\sigma)$ also goes from 0 to l, and $h(\sigma) \geq 0$ so f is nondecreasing.

We can write Eq. (B4) as a Fourier transform [46], by changing variables from σ to f, getting

$$I_x^{(n)} = \frac{1}{l}\int_0^l df\, s(f) e^{i\varpi_n f}\,, \tag{B5}$$

where

$$s(f) = \frac{g(\sigma(f))}{h(\sigma(f))}\,, \tag{B6}$$

and $\sigma(f)$ is the inverse of $f(\sigma)$.

We would like to bound I_x by bounding the derivatives of $s(f)$. We integrate by parts m times in Eq. (B5), finding

$$I_x^{(n)} = \frac{i^m}{l\varpi_n^m}\int_0^l df\, s^{(m)}(x) e^{i\varpi_n x}\,, \tag{B7}$$

where $s^{(m)}$ is the mth derivative of s. If we can bound the derivatives, $|s^{(m)}| < s^{(m)}_{\rm max}$, then we will find $|I_x^{(n)}| < B_m = s^{(m)}_{\rm max}/\varpi_n^m$.

To differentiate $s(f)$, we can take $ds/df = (ds/d\sigma)/(df/d\sigma)$. The effect is to differentiate with respect to σ and then divide by h. We thus have

$$s^{(m)} = \left(h^{-1}\frac{d}{d\sigma}\right)^m \left(h^{-1} g\right)\,. \tag{B8}$$

One term found in $s^{(m)}$ is the one where we repeatedly differentiate the inverse power of h, which thus grows by two units each step, giving

$$s^{(m)} \supseteq \frac{(2m-1)!! h'^m}{h^{-(2m+1)}} g\,. \tag{B9}$$

We conjecture that this is the dominant term. Considering it alone, we can derive a bound. We need to know the largest value of Eq. (B9) anywhere on the string. Since we are not concerning ourselves here with structure in g, we will merely observe that $|g| < 1$. Now $h = 1 - \cos\theta$, where θ is the angle between $\mathbf{x}'$ and the direction of observation. We expect that $|h'| = |X_z''|$ is not too large, because of smoothing. Also when h is small, $\mathbf{X}''$ is mostly transverse to the observation direction. So write

$$s^{(m)}(\sigma) \approx (2m-1)!! \frac{r(\sigma)^m}{h(\sigma)}\,, \tag{B10}$$

where

$$r(\sigma) = \frac{|X_z''(\sigma)|}{h(\sigma)^2}\,. \tag{B11}$$

We're interested in $m \gg 1$, so Eq. (B10) has its maximum at the σ that maximizes r, regardless of m. Let us call this point $\sigma_{\max}$ and let $r_{\max} = r(\sigma_{\max})$. Then

$$B_m = (2m-1)!! \frac{r_{\max}^m}{h(\sigma_{\max})\varpi_n^m} \,. \tag{B12}$$

Ignoring the extra power of h,

$$\ln B_m \approx m(\ln 2m - 1 + \ln(r_{\max}/\varpi_n)) \,, \tag{B13}$$

which is minimized at $m = \varpi_n/(2r_{\max})$, at which point

$$B_m \approx e^{-m} = e^{-\varpi_n/(2r_{\max})} \,. \tag{B14}$$

Thus $I_x^{(n)}$ falls off as $e^{-\varpi_n/(2r_{\max})}$. For a given string and a given $\hat{\mathbf{\Omega}}$, we scan the string to find $r_{\max}$ for I^+ and I^-. Using Eqs. (45,50) this gives us an exponentially declining bound on $dP_n/d\Omega$ and thus a value of $n_{\max}$ after which the power is insignificant.

When we do the calculation using this $n_{\max}$, we check that indeed the computed $dP_n/d\Omega$ are small for the last few n. Thus the even if the conjecture above is not correct, we have good reason to believe that we are not missing any power.

In certain cases, computational resources do not allow us to compute as many harmonics as recommended above. In particular, some loops have "pseudocusps" [53, 54], places where $\mathbf{X}'_+$ and $\mathbf{X}'_-$ come close without crossing. Because such a point is not an actual cusp, it is handled by direct computation, rather than our cusp code. But in observation directions close to $\mathbf{X}'_+$ and $\mathbf{X}'_-$, h is very small and thus $r_{\max}$ large for both I^+ and I^-, so the power remains high for many harmonics. We limit the computation to 10^7 harmonics, so we miss $n > 10^7$ power coming from such regions. This leads to a fictitious drop in the computed power spectrum at $n = 10^7$, as shown in Figs. 3 and 4. This is of much less significance than it appears in the figures, because the actual power is multiplied by $n^{-4/3}$ over what is shown there.

Appendix C: Numerical summation of an infinite series

In this appendix we discuss the computation of an infinite sum,

$$\sum_{n=1}^{\infty} A_n \,, \tag{C1}$$

such as appears in Eq. (6). Of course the A_n must decrease rapidly enough so that the sum converges. We can evaluate only a finite number of A_n, and we must get from there to an approximation for the infinite sum.

A great deal has been written on the subject of numerical integration, but much less on numerical summation. Most of what there is involves the Euler-Maclaurin formula, which enables one to convert a sum of discrete samples of a smooth function into an integral. But here we do not have samples of a smooth function but rather a function defined only at discrete values n. Thus we will develop a little of the needed techniques for numerical summation by analogy with numerical integration.

A numerical integration method can be though of as a way of taking a finite number of samples of the integrand, producing from those an approximation to the integrand, and integrating that instead. For example, in the trapezoidal rule, the integrand is approximated by linear interpolation between sampled points. We will use a similar technique here.

The standard procedure for integrals going to infinity (for example see Ref. [55]) is to perform a change of variable to render the integration range finite. For example if one has

$$\int_1^\infty dx\, f(x)\,, \tag{C2}$$

one can let $t = 1/x$ to get

$$\int_0^1 dt\, f(1/t)/t^2\,. \tag{C3}$$

If $f(x)$ decreases at least as fast as $1/x^2$ [55], then $f(t)/t^2$ will be bounded as $t \to 0$.

In our case, $A_n = C_n P_n$. For very large n, the power P_n is dominated by cusp emission and goes as $n^{-4/3}$. The coefficients C_n decrease, so A_n decreases at least as $n^{-4/3}$ but not necessarily faster. If we had $f(x)$ going as $x^{-4/3}$ in Eq. (C2), we should change variables to $t = x^{-1/3}$, giving

$$3\int_0^1 dt\, f\left(t^{-3}\right)/t^4\,, \tag{C4}$$

where the integrand is bounded as $t \to 0$.

We will now use Eq. (C4) as a guide to approximate Eq. (C1) using a finite number of n. The discrete approximation to the integrand in Eq. (C4) is $S_n = n^{4/3} A_n$, and it is this S_n that we will interpolate between computed values. Furthermore the variable of interpolation, analogous to t, should be $n^{-1/3}$. Thus if we have computed S_n and S_m, we will find S_l for $l \in (m, n)$ by

$$S_l = \frac{m^{-1/3} - l^{-1/3}}{m^{-1/3} - n^{-1/3}} S_n + \frac{l^{-1/3} - n^{-1/3}}{m^{-1/3} - n^{-1/3}} S_m\,. \tag{C5}$$

The sum of terms from m through $n-1$ is given by

$$\sum_{l=m}^{n-1} n^{-4/3} S_l = \frac{S_m - S_n}{m^{-1/3} - n^{-1/3}} [\zeta(5/3, m) - \zeta(5/3, n)] \tag{C6}$$
$$- \frac{n^{-1/3} S_m - m^{-1/3} S_n}{m^{-1/3} - n^{-1/3}} [\zeta(4/3, m) - \zeta(4/3, n)] \,,$$

where

$$\zeta(s, m) = \sum_{k=0}^{\infty} (m + k)^{-s} \tag{C7}$$

is the Hurwitz ζ function.

Suppose we have computed S_n for some set of n_j, $j = 1 \ldots N$. For simplicity, let us require that $n_N = \infty$. Of course $A_\infty = 0$, but if C_n approaches a nonzero limit as $n \to \infty$, then S_∞ is a constant that we can compute, and using it improves the approximation. This occurs when we compute the total power Γ, where $C_n = 1$.

We can write

$$\sum_{n=1}^{\infty} A_n = \sum_{n=1}^{\infty} n^{-4/3} S_n = \sum_{j=1}^{N-1} \sum_{l=n_j}^{n_{j+1}-1} l^{-4/3} S_l \approx \sum_{j=1}^{N} c_j S_{n_j} \,, \tag{C8}$$

where c_j is the sum of the coefficient of S_m in Eq. (C6) with $m = n_j$, $n = n_{j+1}$ and the coefficient of S_n in Eq. (C6) with $m = n_{j-1}$, $n = n_j$,

$$c_j = \frac{\zeta(5/3, n_j) - \zeta(5/3, n_{j+1}) - [\zeta(4/3, n_j) - \zeta(4/3, n_{j+1})] n_{j+1}^{-1/3}}{n_j^{-1/3} - n_{j+1}^{-1/3}} \tag{C9}$$
$$- \frac{\zeta(5/3, n_{j-1}) - \zeta(5/3, n_j) - [\zeta(4/3, n_{j-1}) - \zeta(4/3, n_j)] n_{j-1}^{-1/3}}{n_{j-1}^{-1/3} - n_j^{-1/3}} \,.$$

For $j = 1$, there is no contribution from the previous interval. For $j = N$, there is no contribution from the next interval.

Equation (C5) still holds with $n = \infty$ and consequently $n^{-1/3} = 0$. Then Eq. (C9) holds also. For c_{N-1}, everything vanishes in the first line except the first terms in the numerator and the denominator, while the second line is normal. For c_N the first line is absent because it is the last interval, and in the second line all terms involving n_j vanish.

One might approximate an integral such as Eq. (C4) by evaluating the integrand at evenly spaced t. By analogy, we can choose the n_j so that the $n_j^{-1/3}$ are evenly spaced, as much as possible. We do this by picking a fiducial number N', in our case 1000, choosing $t_i = i/N'$ for $i = 0 \ldots N'$, and letting $\{n_j\}$ be the distinct integers, plus infinity, found by rounding the t_i^{-3}. The number of such modes is about $4(N'/3)^{3/4}$. In our case $N = 312$.

Appendix D: Handling of rare bursts

The above computation of $\Omega_{\rm gw}$ is the computation of its average value. If what we observe is the total contribution due to many loops, then by the central limit theorem we should expect a Gaussian background. But if the average is dominated by a few rare bursts, so rare that we might not have seen any of them, then we should expect a smaller signal. Thus rare bursts should be excluded from the background calculation [34].

Suppose an experiment runs for time T and reports the average signal at some typical frequency f. If strong bursts occur less often than the duration of the experiment, then we would probably not have seen even one, so their contribution should be excluded from our estimate of the average power. So the question is whether any significant contribution to $\Omega_{\rm gw}$ comes from strong bursts that typically do not occur within a time interval T. We will see below that it does not.

One can also consider the status of bursts that occur with frequency greater than $1/T$ but less than frequency f. This might matter for experiments such as LIGO and LISA, but not for pulsar timing, where the typical frequency is about the inverse of the observation time. Bursts with these intermediate rates contribute to the average power over the entire interval T in the usual way, so if that is the observation with which we compare, they do not need to be excluded. In fact, such bursts are likely to be detected by burst detection pipelines, rather than being reported as part of the background. However, this makes the effect more detectable, not less. So including intermediate-rate bursts makes no mistake in detection through the average power, but neglects the possibility of detection of bursts as bursts. That, however, is the subject of a different body of work, and here we will show that there is no need to exclude burst with rates less than $1/T$.

We will show that rare bursts are not important by analyzing a particular population of bursts that are stronger than those that make significant contributions to the background and nevertheless occur frequently in period T. There are two factors that lead to an energetic burst: large loop length l, and recent emission, i.e., small redshift.

We are concerned with tightly beamed bursts emitted by cusps, which means with radiation at frequencies high compared with the loop oscillation frequency $2/l$. Thus the discrete nature of the loop harmonics is not relevant, and we can consider a continuous form of the power, $P(y)$, with $y = (1+z)fl$, where f is the observed frequency today. We define $P(y)$

to be the power per unit y from the given loop, so the power per unit range of observed frequency is $P(y)dy/df = (1+z)lP(y)$.

We now compute the dependence of the burst energy density on l and z. The period in the emitting frame between burst emissions is proportional to l. Thus we multiply by l to convert the power emitted into the energy permitted per burst. Then we divide by $1+z$ because the energy is decreased by redshifting. Thus the present-day energy of a burst per unit range of observed frequency is proportional to $l^2P(y)$. Since $P(y) \propto y^{-4/3}$ [21], this goes as $l^{2/3}(1+z)^{-4/3}$.

Now we consider beaming. We define an approximate beaming angle θ by setting $\xi_\pm = 1$ in Eq. (A26). Since $\alpha_\pm \sim 1/l$, we find $\theta \sim (l\omega)^{-1/3} \sim y^{-1/3}$. Beaming thus enhances the burst energy density by a factor of $\theta^2 \sim y^{2/3}$, giving in all $l^{4/3}(1+z)^{-2/3}$.

In addition, the energy of the burst is diluted by the square of the proper distance to the point of emission, which is proportional to z for $z \ll 1$ and asymptotes to the horizon distance for large z. Again, recent bursts are stronger.

Since recent bursts from large loops are the strongest, we will consider bursts coming from strings of length around some specific $l > \Gamma G\mu t_0$ at places with $z < 1$. Even these large loops are dominated by radiation-era relics, so we can use Eq. (32), with $G_1 = 1$, $z \ll 1$, and $l > \Gamma G\mu t_0$,

$$\mathsf{n}_r(l, t_0) \approx \frac{0.5(H_r^2)^{3/4}}{l^{5/2}}\,. \tag{D1}$$

Using Eq. (15), we find the number of loops per logarithmic interval in l,

$$l\mathsf{n}_r(l, t_0) \approx 9.3 \times 10^9 \left(\frac{l}{\mathrm{yr}}\right)^{-3/2} \mathrm{Gpc}^{-3}\,. \tag{D2}$$

The proper distance to $z = 1$ is about 3.3 Gpc [56], so the volume is $150\mathrm{Gpc}^3$, and the total number of loops

$$N(\ln l) \approx 1.4 \times 10^{12} \left(\frac{l}{\mathrm{yr}}\right)^{-3/2}\,. \tag{D3}$$

Almost all our smoothed loops have 2 cusps per oscillation, so each loop produces bursts at rate $4/l$. The fraction of bursts we can see is given by the fraction of solid angle occupied by the beam, $\theta^2/4$, where, as before, $\theta \approx (fl)^{-1/3}$. Thus the rate of bursts received from a population of loops with lengths around l and $z < 1$ is

$$R = 1.4 \times 10^{12} \left(\frac{l}{\mathrm{yr}}\right)^{-19/6} (f \cdot \mathrm{yr})^{-2/3}\,\mathrm{yr} = 1.4 \times 10^7 \left(\frac{l}{\mathrm{yr}}\right)^{-19/6} \left(\frac{f}{\mathrm{Hz}}\right)^{-2/3} \mathrm{yr}\,. \tag{D4}$$

For pulsar timing, we take $f = (5\text{yr})^{-1}$ and consider loops around $l = 1000$yr. Then we find about 4×10^7 loops emitting 2×10^5 bursts per year, of which we can see about 0.7%, giving 1400 bursts per year. Even these large loops give frequent events which would be seen as a Gaussian background.

We found [7] that $G\mu < 2 \times 10^{-11}$, so $\Gamma G\mu < 10^{-9}$ and the dominant size of loops today, $\Gamma G\mu t_0$, is no more than 14yr. Thus the loops we just considered with $l \sim 1000$yr contribute a negligible fraction of the total background, and ignoring loops larger than these has no effect.

Turning now to LISA, we choose $f = 10^{-2}$ Hz and consider loops around $l = 100$yr, still several times larger than $\Gamma G\mu t_0$. Then Eq. (D4) gives $R = 140/\text{yr}$, so once again rare bursts do not need to be excluded.

For LIGO, we choose $f = 10^2$ Hz and consider loops around $l = 14$yr, finding $R = 150/\text{yr}$. Thus loops right at $\Gamma G\mu t_0$ do not need to be excluded, but significantly larger ones might. But this is very far from making a difference to the background seen by LIGO, which comes almost entirely from emission during the radiation era. Even excluding all matter-era emission would make little difference.

---

[1] A. Vilenkin and E. P. S. Shellard, *Cosmic Strings and Other Topological Defects* (Cambridge University Press, 2000).

[2] Gia Dvali and Alexander Vilenkin, "Formation and evolution of cosmic D strings," JCAP **0403**, 010 (2004), arXiv:hep-th/0312007 [hep-th].

[3] Edmund J. Copeland, Robert C. Myers, and Joseph Polchinski, "Cosmic F and D strings," JHEP **06**, 013 (2004), arXiv:hep-th/0312067 [hep-th].

[4] Jose J. Blanco-Pillado, Ken D. Olum, and Benjamin Shlaer, "Large parallel cosmic string simulations: New results on loop production," Phys. Rev. **D83**, 083514 (2011), arXiv:1101.5173 [astro-ph.CO].

[5] Jose J. Blanco-Pillado, Ken D. Olum, and Benjamin Shlaer, "Cosmic string loop shapes," Phys. Rev. **D92**, 063528 (2015), arXiv:1508.02693 [astro-ph.CO].

[6] Jose J. Blanco-Pillado, Ken D. Olum, and Benjamin Shlaer, "The number of cosmic string loops," Phys. Rev. **D89**, 023512 (2014), arXiv:1309.6637 [astro-ph.CO].

[7] Jose J. Blanco-Pillado, Ken D. Olum, and Xavier Siemens, "New limits on cosmic strings from gravitational wave observation," (2017), arXiv:1709.02434 [astro-ph.CO].

[8] David P. Bennett and Francois R. Bouchet, "Evidence for a Scaling Solution in Cosmic String Evolution," Phys. Rev. Lett. **60**, 257 (1988).

[9] Bruce Allen and E. P. S. Shellard, "Cosmic string evolution: a numerical simulation," Phys. Rev. Lett. **64**, 119–122 (1990).

[10] Vitaly Vanchurin, Ken Olum, and Alexander Vilenkin, "Cosmic string scaling in flat space," Phys. Rev. **D72**, 063514 (2005), arXiv:gr-qc/0501040 [gr-qc].

[11] Christophe Ringeval, Mairi Sakellariadou, and Francois Bouchet, "Cosmological evolution of cosmic string loops," JCAP **0702**, 023 (2007), arXiv:astro-ph/0511646 [astro-ph].

[12] Vitaly Vanchurin, Ken D. Olum, and Alexander Vilenkin, "Scaling of cosmic string loops," Phys. Rev. **D74**, 063527 (2006), arXiv:gr-qc/0511159 [gr-qc].

[13] C. J. A. P. Martins and E. P. S. Shellard, "Fractal properties and small-scale structure of cosmic string networks," Phys. Rev. **D73**, 043515 (2006), arXiv:astro-ph/0511792 [astro-ph].

[14] Ken D. Olum and Vitaly Vanchurin, "Cosmic string loops in the expanding Universe," Phys. Rev. **D75**, 063521 (2007), arXiv:astro-ph/0610419 [astro-ph].

[15] Andreas Albrecht and N. Turok, "Evolution of Cosmic Strings," Phys. Rev. Lett. **54**, 1868–1871 (1985).

[16] Ken D. Olum and J. J. Blanco-Pillado, "Field theory simulation of Abelian Higgs cosmic string cusps," Phys. Rev. **D60**, 023503 (1999), arXiv:gr-qc/9812040 [gr-qc].

[17] J. N. Moore and E. P. S. Shellard, "On the evolution of Abelian Higgs string networks," (1998), arXiv:hep-ph/9808336 [hep-ph].

[18] Ken D. Olum and J. J. Blanco-Pillado, "Radiation from cosmic string standing waves," Phys. Rev. Lett. **84**, 4288–4291 (2000), arXiv:astro-ph/9910354 [astro-ph].

[19] A. Vilenkin, "Gravitational radiation from cosmic strings," Phys. Lett. **107B**, 47–50 (1981).

[20] C. J. Hogan and M. J. Rees, "Gravitational interactions of cosmic strings," Nature **311**, 109–113 (1984).

[21] Tanmay Vachaspati and Alexander Vilenkin, "Gravitational Radiation from Cosmic Strings," Phys. Rev. **D31**, 3052 (1985).

[22] Frank S. Accetta and Lawrence M. Krauss, "The stochastic gravitational wave spectrum resulting from cosmic string evolution," Nucl. Phys. **B319**, 747–764 (1989).

[23] David P. Bennett and Francois R. Bouchet, "Constraints on the gravity wave background generated by cosmic strings," Phys. Rev. **D43**, 2733–2735 (1991).

[24] R. R. Caldwell and Bruce Allen, "Cosmological constraints on cosmic string gravitational radiation," Phys. Rev. **D45**, 3447–3468 (1992).

[25] Xavier Siemens, Vuk Mandic, and Jolien Creighton, "Gravitational wave stochastic background from cosmic (super)strings," Phys. Rev. Lett. **98**, 111101 (2007), arXiv:astro-ph/0610920 [astro-ph].

[26] Matthew R. DePies and Craig J. Hogan, "Stochastic Gravitational Wave Background from Light Cosmic Strings," Phys. Rev. **D75**, 125006 (2007), arXiv:astro-ph/0702335 [astro-ph].

[27] S. Olmez, V. Mandic, and X. Siemens, "Gravitational-Wave Stochastic Background from Kinks and Cusps on Cosmic Strings," Phys. Rev. **D81**, 104028 (2010), arXiv:1004.0890 [astro-ph.CO].

[28] S. A. Sanidas, R. A. Battye, and B. W. Stappers, "Constraints on cosmic string tension imposed by the limit on the stochastic gravitational wave background from the European Pulsar Timing Array," Phys. Rev. **D85**, 122003 (2012), arXiv:1201.2419 [astro-ph.CO].

[29] Sotirios A. Sanidas, Richard A. Battye, and Benjamin W. Stappers, "Projected constraints on the cosmic (super)string tension with future gravitational wave detection experiments," Astrophys. J. **764**, 108 (2013), arXiv:1211.5042 [astro-ph.CO].

[30] Pierre Binetruy, Alejandro Bohe, Chiara Caprini, and Jean-Francois Dufaux, "Cosmological Backgrounds of Gravitational Waves and eLISA/NGO: Phase Transitions, Cosmic Strings and Other Sources," JCAP **1206**, 027 (2012), arXiv:1201.0983 [gr-qc].

[31] Sachiko Kuroyanagi, Koichi Miyamoto, Toyokazu Sekiguchi, Keitaro Takahashi, and Joseph Silk, "Forecast constraints on cosmic string parameters from gravitational wave direct detection experiments," Phys. Rev. **D86**, 023503 (2012), arXiv:1202.3032 [astro-ph.CO].

[32] Sachiko Kuroyanagi, Koichi Miyamoto, Toyokazu Sekiguchi, Keitaro Takahashi, and Joseph Silk, "Forecast constraints on cosmic strings from future CMB, pulsar timing and gravitational wave direct detection experiments," Phys. Rev. **D87**, 023522 (2013), [Erratum: Phys. Rev.D87,no.6,069903(2013)], arXiv:1210.2829 [astro-ph.CO].

[33] Thibault Damour and Alexander Vilenkin, "Gravitational wave bursts from cosmic strings," Phys. Rev. Lett. **85**, 3761–3764 (2000), arXiv:gr-qc/0004075 [gr-qc].

[34] Thibault Damour and Alexander Vilenkin, "Gravitational wave bursts from cusps and kinks

on cosmic strings," Phys. Rev. **D64**, 064008 (2001), arXiv:gr-qc/0104026 [gr-qc].

[35] Thibault Damour and Alexander Vilenkin, "Gravitational radiation from cosmic (super)strings: Bursts, stochastic background, and observational windows," Phys. Rev. **D71**, 063510 (2005), arXiv:hep-th/0410222 [hep-th].

[36] Xavier Siemens, Jolien Creighton, Irit Maor, Saikat Ray Majumder, Kipp Cannon, and Jocelyn Read, "Gravitational wave bursts from cosmic (super)strings: Quantitative analysis and constraints," Phys. Rev. **D73**, 105001 (2006), arXiv:gr-qc/0603115 [gr-qc].

[37] C. J. Moore, R. H. Cole, and C. P. L. Berry, "Gravitational-wave sensitivity curves," Class. Quant. Grav. **32**, 015014 (2015), arXiv:1408.0740 [gr-qc].

[38] P. A. R. Ade *et al.* (Planck), "Planck 2015 results. XIII. Cosmological parameters," Astron. Astrophys. **594**, A13 (2016), arXiv:1502.01589 [astro-ph.CO].

[39] Jeremy M. Wachter and Ken D. Olum, "Gravitational smoothing of kinks on cosmic string loops," Phys. Rev. Lett. **118**, 051301 (2017), arXiv:1609.01153 [gr-qc].

[40] Jeremy M. Wachter and Ken D. Olum, "Gravitational backreaction on piecewise linear cosmic string loops," Phys. Rev. **D95**, 023519 (2017), arXiv:1609.01685 [gr-qc].

[41] T. W. B. Kibble and Neil Turok, "Selfintersection of Cosmic Strings," Phys. Lett. **116B**, 141–143 (1982).

[42] Neil Turok, "Grand Unified Strings and Galaxy Formation," Nucl. Phys. **B242**, 520–541 (1984).

[43] David Garfinkle and Tanmay Vachaspati, "Radiation From Kinky, Cuspless Cosmic Loops," Phys. Rev. **D36**, 2229 (1987).

[44] Kendall Atkinson, "Numerical integration on the sphere," J. Austral. Math. Soc. (Series B) **23**, 332–347 (1982).

[45] C. J. Burden, "Gravitational Radiation From a Particular Class of Cosmic Strings," Phys. Lett. **164B**, 277–281 (1985).

[46] Bruce Allen and E. P. S. Shellard, "Gravitational radiation from cosmic strings," Phys. Rev. **D45**, 1898–1912 (1992).

[47] Bruce Allen and Adrian C. Ottewill, "Wave forms for gravitational radiation from cosmic string loops," Phys. Rev. **D63**, 063507 (2001), arXiv:gr-qc/0009091 [gr-qc].

[48] D. Potts, G. Steidl, and M. Tasche, "Fast fourier transforms for nonequispaced data: A tutorial," in *Modern Sampling Theory: Mathematics and Applications*, edited by J. J. Benedetto

and P. Ferreira (Birkhauser Basel, 2001) pp. 253–274.

[49] Bruce Allen, Paul Casper, and Adrian Ottewill, "Analytic results for the gravitational radiation from a class of cosmic string loops," Phys. Rev. **D50**, 3703–3712 (1994), arXiv:gr-qc/9405037 [gr-qc].

[50] Malcolm R. Anderson, "Self-similar evaporation of a rigidly-rotating cosmic string loop," Class. Quant. Grav. **22**, 2539–2568 (2005), arXiv:gr-qc/0505160 [gr-qc].

[51] Malcolm Anderson, "Continuous self-similar evaporation of a rotating cosmic string loop," Class. Quant. Grav. **26**, 025006 (2009), arXiv:0812.2523 [gr-qc].

[52] Malcolm Anderson, "Gravitational waveforms from the evaporating ACO cosmic string loop," Class. Quant. Grav. **26**, 075018 (2009), arXiv:0903.4943 [gr-qc].

[53] Thomas Elghozi, William Nelson, and Mairi Sakellariadou, "Cusps and pseudocusps in strings with Y-junctions," Phys. Rev. **D90**, 123517 (2014), arXiv:1403.3225 [hep-th].

[54] Matthew J. Stott, Thomas Elghozi, and Mairi Sakellariadou, "Gravitational Wave Bursts from Cosmic String Cusps and Pseudocusps," Phys. Rev. **D96**, 023533 (2017), arXiv:1612.07599 [hep-th].

[55] William H. Press, Saul A. Teukolsky, William T. Vetterling, and Brian P. Flannery, *Numerical Recipes: The Art of Scientific Computing*, 3rd ed. (Cambridge University Press, New York, NY, USA, 2007).

[56] Edward L. Wright, "A Cosmology Calculator for the World Wide Web," Publ. Astron. Soc. Pac. **118**, 1711–1715 (2006), arXiv:astro-ph/0609593 [astro-ph].